Journal of Marine Science and Application (2026) 25: 491-507
https://doi.org/10.1007/s11804-025-00702-8

RESEARCH ARTICLE

Dynamic Response of Triceratops with Elliptical Legs under Oblique Space Launches

Srinivasan Chandrasekaran[1] and Puliparambil Unnikrishnan Ashish[1]

Received: 16 December 2024 / Accepted: 05 March 2025

Abstract

The offshore triceratops platform has emerged as a promising candidate for maritime launches due to its innovative and unique responsive characteristics. Their form-dominant design facilitates dynamic equilibrium and effectively controls the impact of the deck's rotational motion during sea-borne launch. A parametric study examines how the shape of buoyant legs influences the dynamic response during rocket launches, utilizing ANSYS AQWA for analysis. The study finds that elliptical legs with an eccentricity of 2 reduce deck responses. While the deck rotation is driven by the quasi-static rocket thrust and the differential heave of the legs, the pitch response arises from the waves and is reduced by using elliptical legs. Numerical studies conducted during rocket launches show an amplified deck response. The vertical force on the deck is maximized during vertical launches and minimized during 30° launches. The pitch moment on the deck increases with launch eccentricity, which is attributed to the cantilever effect of the launch platform.

Keywords Triceratops; Marine space launch; Elliptical legs; Oblique rocket launch; Dynamic analysis; Form dominant response control; Compliant platform

1 Introduction

The major and traditional function of an offshore platform has been oil and gas exploration and production (Li and Hu, 2022). However, recent research has shifted focus to leveraging marine conditions for sustainable and environmentally friendly space launches. In addition to meeting the required orbital inclination (Seumahu, 1997) with minimal fuel consumption (Cashin, 2001), launching from marine platforms also mitigates potential risks to populated areas in case of launch mishaps. Consequently, the domain of space launches has witnessed a shift from land-based to marine launches. However, rockets launched from offshore platforms may potentially affect the structural integrity of the platform due to the additional impact and heat effects. Prolonged exposure to high-intensity fire could undermine the load capacity of the platform. Geometrically dominant designs, also called form-dominant, are highly effective in counteracting the applied lateral loads (Shabanlou et al., 2021; Chandrasekaran et al., 2021; Chandrasekaran, 2017). Researchers and industry professionals have explored various offshore structures for launch activities, leveraging their distinct advantages. Fixed platforms provide stability and cost-effectiveness in shallower waters (Ahmad, 2021b; Amiri et al., 2021), while floating platforms, known for their adaptability and versatility, are more suited for deeper and remote offshore locations (Ahmad, 2021a). Compliant platforms, such as tension leg platforms (TLPs), are designed to be more flexible in response to external loads compared to fixed offshore platforms (Chen and Zhang, 2017; Johnson et al., 1993; Li and Kareem, 1992). Notably, resonance in their flexible degrees of freedom is unlikely due to their higher natural periods than the wave period (Jain, 1997).

Offshore launch technology has advanced from the use of fixed offshore platforms for marine launches (Caporale, 1968) to semi-submersible self-propelled platforms designed for launching large rockets (Song et al., 2021; Draim, 1993). Semi-submersibles offer a solution to the limitations of fixed structures (Frieze et al., 1997) for launching large rockets because they are self-propelled platforms deployable in

Article Highlights

- Elliptical legs reduce surge, sway, heave, roll, and pitch with the best sway and pitch responses observed at an eccentricity of 2.
- Wave forces primarily drive surge and sway, while differential heave between legs influences deck heave, roll, and pitch.
- Wave-induced moments are more significant on the buoyant legs, while rocket launch moments are more significant on the deck, with limited transfer due to joint articulation.
- Vertical launches exert the highest force on the deck, whereas 30° launches result in the lowest deck force.

✉ Srinivasan Chandrasekaran
drsekaran@iitm.ac.in

[1] Dept. of Ocean Engineering, Indian Institute of Technology, Madras 600036, India

deeper seas (Buhrig, 1996). These structures are preferred among neutrally buoyant floating structures due to their superior hydrodynamic characteristics (Fu et al., 2018). Studies on drillships equipped with launch facilities confirm their adaptability for space research (Pang et al., 2023). However, integrating the deck with the hull in a monolithic manner means that the loads from rocket launches directly affect the hull. Consequently, the hull must be specifically designed to withstand these large loads, thereby increasing construction and maintenance costs. Additionally, metocean-induced loads on the hull are transferred to the deck, potentially destabilizing the launch pad and compromising the safe and reliable launch of rockets. Similar challenges arise with structures such as spars and TLPs, primarily due to the rigid connection between the hull and the launch deck. Dynamic analyses conducted by researchers showcased the advantages of the form-dominant design and its innovative positively buoyant "triceratops" (White et al., 2005; Chandrasekaran and Madhuri, 2015). Chauhan et al. demonstrated the superiority of the Triceratops design over conventional spars in deep-ocean environments (Chauhan et al., 2024). The partial isolation of the legs from the deck offers an advantage in exploring maritime-based rocket launches in deep-sea environments (Chandrasekaran and Nagavinothini, 2019; Lin et al., 1990). This isolation helps improve the self-centering capability of the system (Li et al., 2017). Recent studies have highlighted the enhanced structural performance and response advantages over conventional marine-launching structures (Ashish et al., 2024). With the restrained transfer of responses and impact forces from the deck to the buoyant legs, the partially isolated compliant platform exhibited a stiff response in the vertical plane, proving that Triceratops is a viable candidate for sea-based rocket launches.

The rotational motion of the deck considerably affects the effectiveness of sea-borne launches. Therefore, reducing the responses of the deck is crucial for ensuring the suitability of the platform for launch operations. The designs of stiffened triceratops help reduce deck motion in deep-sea conditions by improving their recentering capabilities (Chandrasekaran and Mayank, 2017). Nagavinothini and Chandrasekaran (2020) investigated the impact of elliptical legs on the response of the triceratops platform. Mass slider systems and tuned mass dampers effectively control these responses (Zhang and Li, 2021). Motion instability in floating structures is one of the main concerns, particularly when assessing their performance during hurricane sea states (Chandrasekaran et al., 2023; Chandrasekaran et al., 2021). Offshore triceratops platforms operate in a dynamic equilibrium state, increasing their susceptibility to instability induced by eccentric and oblique launches from the deck. The present study examines the response characteristics and forces experienced by the structure during various oblique and eccentrical vertical launches, alongside the structural response and force analysis of the elliptical leg triceratops during rocket launch operations.

2 Numerical analysis

2.1 Rigid body dynamics

An offshore triceratops platform comprises buoyant columns connected to the topside using ball and socket joints (Figure 1). This platform restrains rotation but transfers translational motion to the topside. The triceratops platform features a triangular deck supported by three buoyant legs. Considering its positive buoyancy, the platform is highly stiff in roll, pitch, and heave motions but remains flexible in sway, yaw, and surge motions. A rocket launch from an offshore triceratops has 12 degrees of freedom: three each for three legs and three for the topside. The deck rotation is independent of the hull's roll, pitch, and yaw due to the ball and socket joints. The ball-and-socket joint mechanism (Figure 2) plays a crucial role in limiting excessive motion of the offshore platform, particularly during dynamic loading conditions. By allowing independent rotational motion while enabling shared translational movement between the topside and the buoyant legs, the ball joints reduce the transmission of moments that could cause excessive topside motion.

All the salient features of the rocket launching structure and the associated idealizations are elaborated by Ashish et al. (2024), along with the mathematical formulation leading to the solution using the average acceleration method. The platform is numerically designed based on the parameters provided in Tables 1–4. The hydrostatic stability of the resulting structure is confirmed by its metacentric height, which is 51.38 m. As shown in Figure 1, an extended deck has been chosen for conducting launching activities away from the production activity zone, ensuring the safety and integrity of the rocket launch mission.

The numerical model is created in ANSYS, as shown in Figure 3. The legs are designed as line elements, whereas the deck is modeled as a surface element. A rocket with a thrust force of 2 500 kN and a base time of 0.8 s is launched from the extended portion of the deck. Tethers, under high axial pretension, connect the hull to the seabed. The high axial stiffness of the tethers ensures rigid body motion in the vertical plane. Triceratops are high-buoyancy structures; thus, tethers play a crucial role in making the triceratops platform suitable for production and launch activities. Initially, a response analysis is conducted on a Triceratops with circular legs. Subsequently, the leg eccentricity is varied by using three types of elliptical legs: eccentricity, $e = 1.5$, $e = 2$, and $e = 2.5$. The study defines leg eccentricity as the ratio of the length of the major axis to the minor axis. Hence, for circular legs, the ratio is unity. The dimensions of the various leg types are shown in Figure 4.

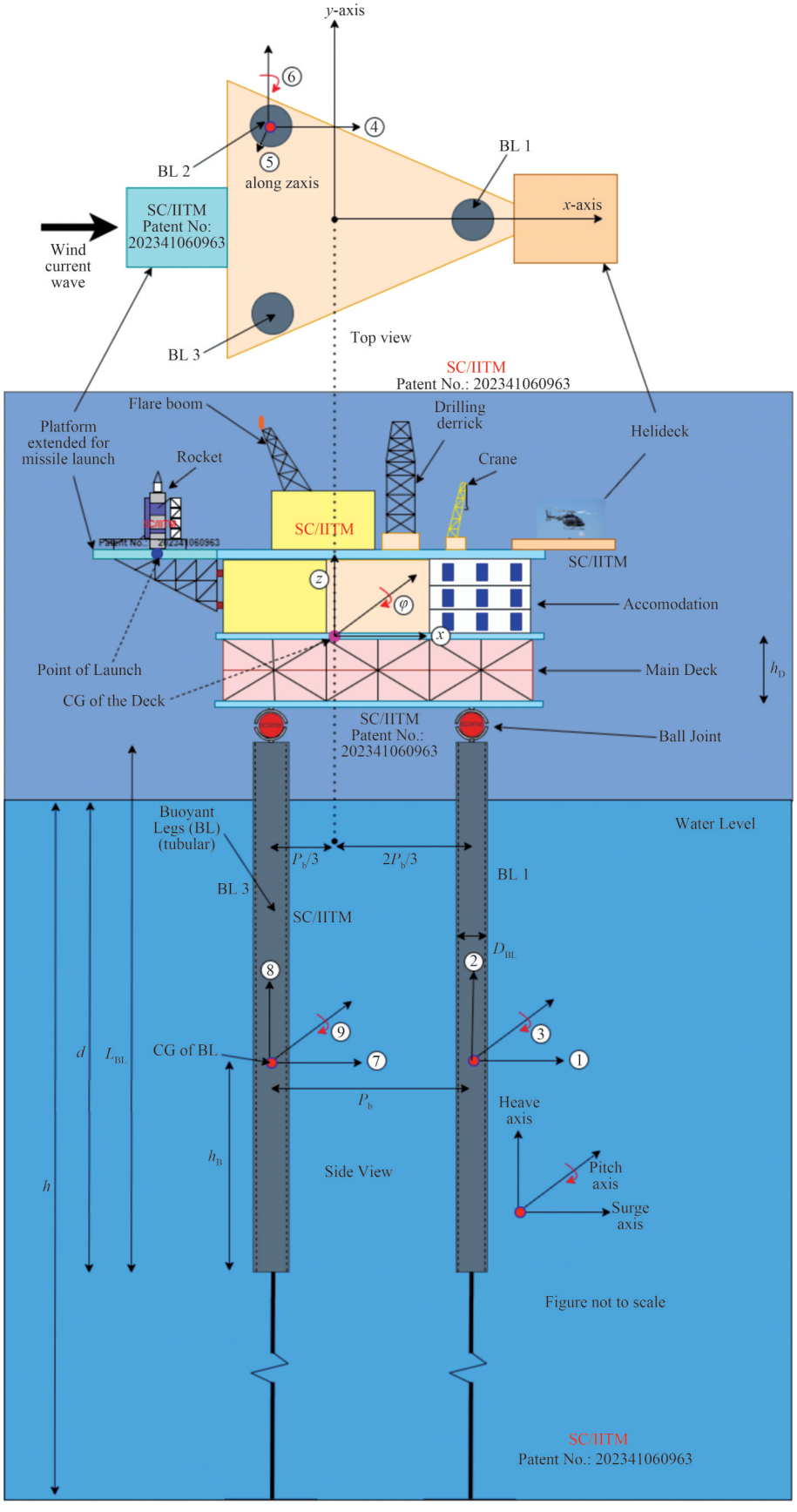

Figure 1 Conceptual model of rocket launching triceratops[patented] platform (Patent No.: 202341060963)

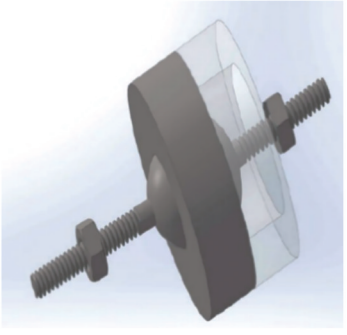

Figure 2 Conceptual model of ball and socket joint (Chandrasekaran and Mayanak, 2016)

Table 1 Structural details of the deck with a rocket launcher (Ashish et al., 2024)

Description	Details
Material	steel
Shape of deck	triangular
Length of deck (m)	95
Depth of dec (m)	12
Area of deck (m^2)	3933
Deck weight + payload (MN)	187.56
Center of mass about the x-axis, CM_x (m)	0
Center of mass about the y-axis, CM_y (m)	0
Center of mass about the z-axis, CM_z (m)	26.24
Radius of gyration about the x-axis, K_{xx} (m)	19.64
Radius of gyration about the y-axis, K_{yy} (m)	19.64
Radius of gyration about the z-axis, K_{zz} (m)	27.43
Weight of extended platform (MN)	0.98
Extended platform CM_x (m)	−34.92
Extended platform CM_y (m)	0
Extended platform CM_z (m)	31.24
Extended platform K_{xx} (m)	4.86
Extended platform K_{yy} (m)	4.86
Extended platform K_{zz} (m)	6.73

Table 2 General structural details of buoyant leg (Ashish et al., 2024)

Description	Details
Material	steel
Shape of leg	circular
Number of legs	3
Diameter of leg (D_{BL}, m)	15
c/c distance between legs (P_b, m)	61.77
Length of the buoyant leg (L_{BL}, m)	174.24
Freeboard (m)	20.24
Draft (d, m)	154
Meta-centric height (m)	51.38
Unit weight of steel (kg/m^3)	7850
Weight of legs (MN)	75
Ballast weight (MN)	309
Buoyancy per leg (MN)	280.75

Table 3 Center of mass and radius of gyration of specific buoyant legs (Ashish et al., 2024) m

Description	CM_x	CM_y	CM_z	K_{xx}	K_{yy}	K_{zz}
Leg 1	35.66	0	−67.88	51.54	51.54	7.29
Leg 2	−17.83	30.89	−67.88	51.54	51.54	7.29
Leg 3	−17.83	−30.89	−67.88	51.54	51.54	7.29

Table 4 Center of mass and radius of gyration of the ballast on buoyant leg (Ashish et al., 2024) m

Description	CM_x	CM_y	CM_z	K_{xx}	K_{yy}	K_{zz}
Ballast 1	35.66	0	−144	15.5	15.5	0
Ballast 2	−17.83	30.89	−144	15.5	15.5	0
Ballast 3	−17.83	−30.89	−144	15.5	15.5	0

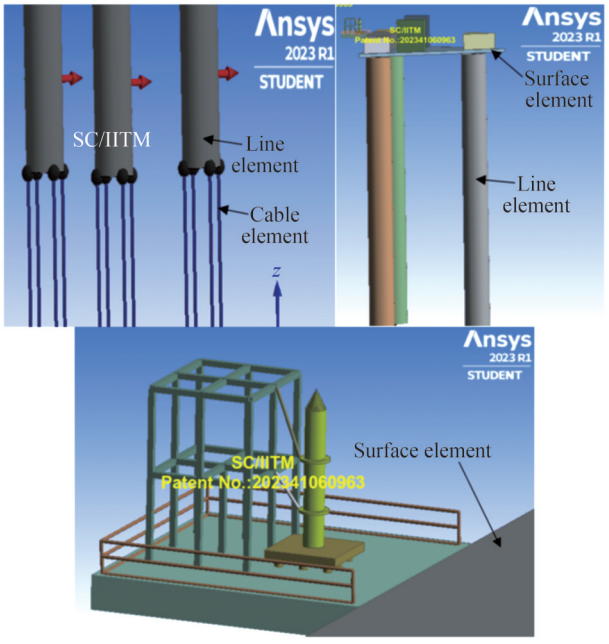

Figure 3 Numerical model of rocket launching triceratops[patented] platform with extended launch platform and tether configurations (Patent No.: 202341060963)

The force equilibrium of a three-legged rocket launching Triceratops (Figure 1) in the vertical plane is given by (Ashish et al., 2024):

$$F_B = W + 3\left(T_T\right) + F_T(t) \tag{1}$$

where F_B is the buoyancy force, W is the sum of the weight of the platform and the payload, T_T is the initial pretension in the tethers, and F_T is the thrust force from the rocket launch. Notably, Triceratops is designed for a high degree of positive buoyancy. The equation of motion is given as:

$$\left(\boldsymbol{M} + \boldsymbol{M}_a\right)\ddot{\boldsymbol{x}} + \boldsymbol{C}\dot{\boldsymbol{x}} + \boldsymbol{K}\boldsymbol{x} = \boldsymbol{F}(t) \tag{2}$$

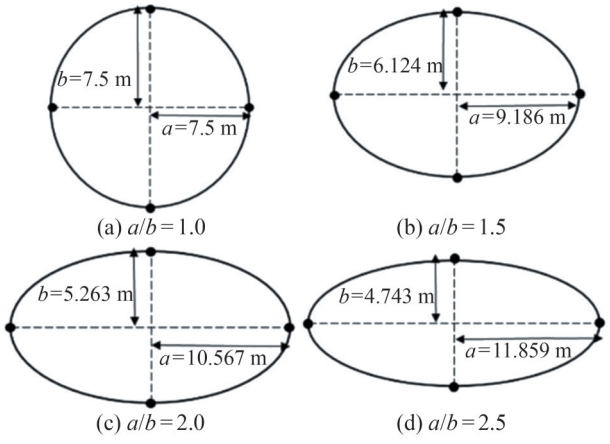

Figure 4 Cross-section of buoyant legs with (a) circular legs, (b) with eccentricity, e = 1.5, (c) e = 2, and (d) e = 2.5 (Nagavinothini and Chandrasekaran, 2020)

where $\boldsymbol{M}$ is the mass matrix, $\boldsymbol{M}_a$ is the added mass matrix, $\boldsymbol{C}$ is the damping matrix, and $\boldsymbol{K}$ is the stiffness matrix of the offshore Triceratops. Furthermore, $\ddot{\boldsymbol{x}}$, $\dot{\boldsymbol{x}}$, and $\boldsymbol{x}$ are the acceleration, velocity, and displacement vectors of the platform in all the degrees of freedom, respectively, while $\boldsymbol{F}(t)$ is the external exciting force. The mass of the platform is the sum of the deck mass, buoyant legs, payload, and rocket load. The added mass, attributed to variable submergence caused by large displacements in flexible degrees of freedom, is considered separately. Chandrasekaran et al. (2013) discussed the derivation of the mass, stiffness, damping, and hydrodynamic coefficients from the rudimentary stage. The exciting force acting on the platform is the sum of the hydrodynamic, $\boldsymbol{F}_w(t)$, and the rocket launch force, $\boldsymbol{R}(t)$. The corresponding matrices are given as follows:

$$\boldsymbol{F}(t) = \boldsymbol{F}_w(t) + \boldsymbol{R}(t) \tag{3}$$

The components of the equation of motion are response-dependent, which is typical for offshore compliant structures and can be solved using the average acceleration method (Newmark, 1959).

2.2 Hydrodynamic and rocket launch forces

Notably, the exciting force is a sum of the hydrodynamic force, $\boldsymbol{F}_w(t)$ and the rocket launch force, $\boldsymbol{R}(t)$, acting on the platform. The hydrodynamic force analysis used linear wave theory, assuming the fluid to be incompressible, inviscid, and governed by irrotational flow. These assumptions are true for deep-water conditions where wave steepness is small. The rocket launch is considered near the Mediterranean Sea, an optimal equatorial launch site. The JONSWAP spectrum generally performs well in the Mediterranean Sea, as well as along the coasts of Portugal and Northern Spain, in the Baltic Sea, and around Iceland and Western Ireland (Mazzaretto et al., 2022). Hence, the numerical study is conducted based on the following met-ocean conditions: the irregular wave follows the Joint North Sea Wave Project (JONSWAP) spectrum, characterized by a substantial wave height of 10 m and a peak period of 13 s. The current velocity starts at 1.65 m/s at the ocean surface, decreases linearly to 1.24 m/s at 34.65 m, and reaches 0 m/s at 69.3 m (Chandrasekaran et al., 2023). Additionally, waves and currents impact the structure at zero degrees, aligned with the surge axis.

$\boldsymbol{R}(t)$ denotes the rocket launching forces, and their influence on the offshore triceratops can be represented in matrix form as follows:

$$\boldsymbol{R}(t)^{\mathrm{T}} = \left\{F_x F_z F_\varphi F_1 F_2 F_3 F_4 F_5 F_6 F_7 F_8 F_9\right\} \tag{4}$$

where subscripts x, z, and φ represent the surge, heave, and pitch degrees of freedom of the topside, respectively, while 1–3, 4–6, and 7–9 represent that of legs 1, 2, and 3, respectively (Figure 1). Furthermore, the surge and heave forces due to the rocket launch are distributed equally over the buoyant legs. Therefore,

$$F_1 = F_4 = F_7 = F_x/3 \tag{5}$$

$$F_2 = F_5 = F_8 = F_z/3 \tag{6}$$

Due to the ball-and-socket joints, the rocket launch does not generate any moment about the center of gravity of the individual legs. Hence,

$$F_3 = F_6 = F_9 = 0 \tag{7}$$

The effect of the inclined rocket thrust forces on the deck center of gravity is illustrated in Figure 5. Using basic mechanics of structures and the force diagram, the remaining force elements can be derived.

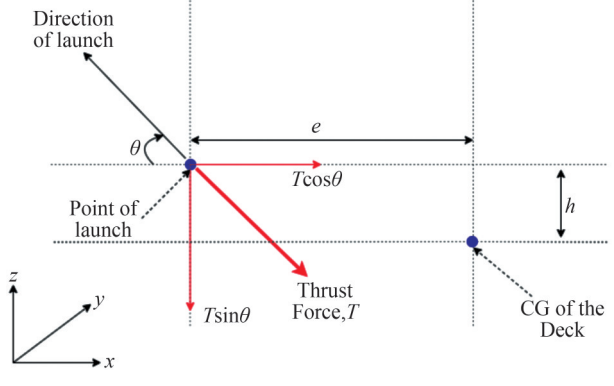

Figure 5 Vector representation of thrust forces in relation to the CG of the deck

Case 1: When the rocket is launched from an eccentricity (e) from the center of gravity of the deck, with a launch angle θ, where $0 < \theta \leqslant 90°$,

$$F_x = T\cos\theta \tag{8}$$

$$F_z = -T\sin\theta \tag{9}$$

$$F_\varphi = T\cos\theta\, h - T\sin\theta\, e \tag{10}$$

where h is half the deck height H, and T is the thrust force of the rocket.

When $\theta = \theta_0$, where $\tan\theta_0 = h/e = H/(2e)$, then the thrust force line passes through the deck's center of gravity, resulting in zero deck pitch.

$$F_x = T\cos\theta_0\,;\ F_z = -T\sin\theta_0\,;\ F_\varphi = 0 \tag{11}$$

When $\theta = 90°$ (the vertical launch case),

$$F_x = 0\,;\ F_z = -T;\ F_\varphi = -Te \tag{12}$$

Case 2: When the rocket is launched from an eccentricity e from the center of deck gravity, with a launch angle θ, where $90° < \theta < 180°$ such that the acute angle ϕ can be represented as $\phi = 180° - \theta$, then

$$F_x = -T\cos\phi \tag{13}$$

$$F_z = -T\sin\phi \tag{14}$$

$$F_\varphi = -T\cos\phi\, h - T\sin\phi\, e \tag{15}$$

Case 3: When the launch eccentricity is zero ($e = 0$), and the launch angle is θ, where $0 < \theta \leqslant 90°$

$$F_x = 0\,;\ F_z = -T;\ F_\varphi = T\cos\theta\, h \tag{16}$$

When $\theta = 90°$,

$$F_x = 0\,;\ F_z = -T;\ F_\varphi = 0 \tag{17}$$

The present study conducts numerical analyses for θ = 30°, 60°, 90°, 120°, 150° and eccentricity e = 0, 10, 20, and 30 m, which are denoted as (A30, A60, A90, A120, A150) and (E0, E10, E20, E30), respectively.

2.3 Quadra log response representation

The response outputs from the numerical analysis are converted into quadra-log plots using Equations (18)–(21). This method effectively portrays the dynamic response characteristics by integrating displacement and its derivatives on a logarithmic scale. Pseudo displacement and pseudo acceleration are depicted along the inclined axes, while the frequency ratio and velocity are represented along the horizontal and vertical axes, respectively. This innovative approach allows for diverse interpretations of the response spectrum. While velocity is measured quantitatively, displacement and acceleration are represented qualitatively. The following characteristic relationship allows for such representation:

$$R_v = \beta R_D \tag{18}$$

$$R_A = \beta R_V = \beta^2 R_D \tag{19}$$

$$\log R_V = \log\beta + \log R_D \tag{20}$$

$$\log R_A = 2\log\beta + \log R_D \tag{21}$$

where R_D, R_V, and R_A are the displacement and its first- and second-time derivatives of the structure at β, which is defined as the ratio of the wave frequency to the structure's natural frequency. Using the methodology outlined by Ashish et al. (2024), the inclined axes are drawn to a uniform scale (in this case, 3), while the vertical and horizontal axes demonstrate a scale of 10. Following the procedures outlined in the literature, quadra-log plots are generated for the vertical plane degrees of freedom, as well as for sway and roll, for the deck and buoyant legs, allowing for comparisons between the responses of all four leg shapes. Logarithmic plots offer the advantage of facilitating accurate comparisons between remarkably large and small values. A quadra-log plot, comprising quadri-points, provides a comprehensive qualitative representation of the dynamic equation of motion. The displacement–velocity–acceleration plot method provides extensive insights into the system's behavior. The data obtained is utilized for structural response analysis, and the quadra-log plot provides engineers with valuable insights into the contributions of displacement and its derivatives at various frequency ratios. For instance, if displacement is a key factor for a specific degree of freedom within a certain frequency range, then adjusting the system's stiffness components can help reduce the overall response. Similarly, if the velocity parameter is dominant, then modifying the damping components can be effective. Therefore, this comprehensive understanding of the response characteristics allows for engineering adjustments to damping, stiffness, and mass, optimizing the response and performance of the elliptical legs rocket launch triceratops under diverse wave conditions. Another advantage of the quadra-logarithmic D–V–A plot lies in its capability to provide insights into the structure's resonance response and its impact on the inertial, damping, and restoring force components.

2.4 Model validation

The developed model is validated by comparing the computed natural periods of the platform's degrees of freedom with results from previous studies (Table 5). The observed difference in the natural period for surge, compared to the reference study, can be attributed to the inclusion of the

additional mass from the extended rocket launch platform and variations in the water depth considered in the analysis. This validation step ensures the reliability of the numerical approach and confirms the suitability of the model for evaluating the dynamic response of rocket-launching offshore platforms.

Table 5 Dynamic characteristics of the deck with the proposed missile launcher

Description	Time period (s)	
	Present study	Reference study (Chandrasekaran and Rao, 2019)
Surge	156.8	133.0
Heave	3.0	3.2
Pitch	3.0	3.1

3 Results and discussions

3.1 Response analysis of deck and elliptical buoyant legs

Figure 6 and Table 6 illustrate the quadra-log deck response spectrum, highlighting the influence of leg eccentricity on surge, sway, heave, roll, and pitch responses. The study reveals that elliptical legs with an eccentricity of 2.5 exhibit the lowest surge response, while legs with an eccentricity of 2 register the lowest sway, heave, roll, and pitch responses. Wave impacts along the surge axis of the legs are directly correlated with the cross-sectional area normal to the surge axis, resulting in higher surge responses for circular cross-sections (Figure 7 and Table 7). This trend is also observed in the deck due to the rigid connection between the topside and hull in translational degrees of freedom. The sway response peaks for legs with circular cross-sections due to the creation of a substantial wake region. As the eccentricity of elliptical legs increases, the wake region size decreases; however, a competing trend emerges where the sway wave impact increases with the cross-sectional area normal to the sway axis. Consequently, legs with an eccentricity of 2.5 have the largest sway cross-sectional area, but they do not exhibit the highest sway response. The optimal minimum sway response is observed in legs with an eccentricity of 2, which balances these competing trends. The heave response is influenced by the vertical stiffness of the legs, which is related to the cross-sectional area of the legs. However, the response varies with leg eccentricity when peak waves are incident, with the minimum heave peak observed for legs with an eccentricity of 2. Similar to the sway response, the maximum roll is recorded for circular legs, attributed to the maximum wake region produced by legs with an eccentricity of 1. However, the magnitude of sway and roll responses is considerably lower

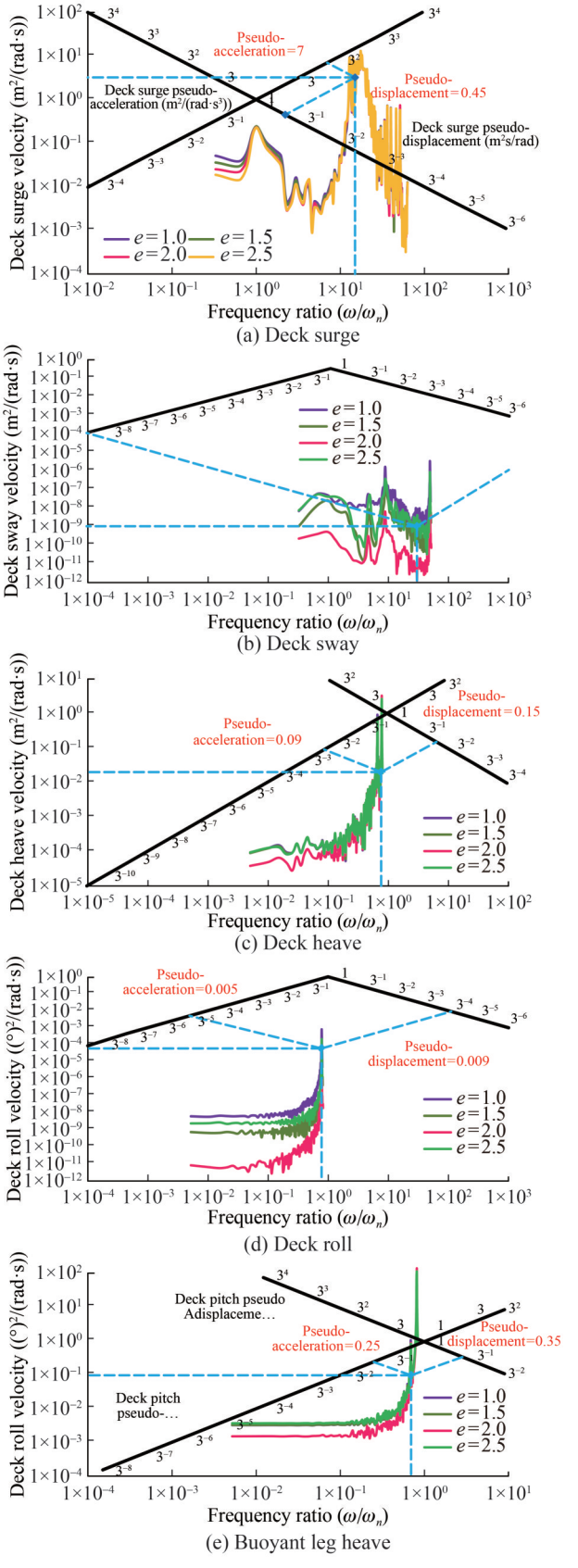

Figure 6 Four-way logarithmic deck responses during rocket launch for various elliptical legs

Table 6 Comparison of the deck responses for various elliptical legs

Leg eccentricity	Deck responses				
	Surge	Sway	Heave	Roll	Pitch
Circular (e = 1)	Max (1)	Max (1)	Max	Max (1)	3
e = 1.5	2	3	Max	3	2
e = 2	3	Min (4)	Min (4)	Min (4)	Min (4)
e = 2.5	Min (4)	2	Max	2	Max (1)

than that of surge, heave, and pitch because the wave is incident parallel to the surge axis. The pitch response of the topside is maximized when the highest eccentricity is used, while the minimum response is observed for legs with an eccentricity of 2. The eccentric pitch moment exerted on the extended topside platform is optimally redistributed when e = 2 is used, resulting in the minimal deck pitch response. The deck pitch is not influenced by leg pitch due to the isolation provided by novel ball joints. Instead, the deck pitch is caused by the rocket launch thrust force and the uneven heave of the hull. Additionally, the pitch response of the legs remains constant, regardless of leg eccentricity. The independent nature of the leg and deck pitch motions is further evidenced by the distinct frequency bands of their responses. Deck pitch exhibits a single peak within a narrow frequency band, whereas leg pitch shows multiple peaks across a wide frequency band. While the leg pitch is produced by the waves, the deck pitch results from the rocket thrust and differential heave of the legs. To ensure robustness during the rocket launch, minimizing deck motion is critical. Legs with an eccentricity of 2 offer optimal performance by reducing sway, heave, and pitch responses, thus providing a stable platform for launch operations.

From the quadra-log plots for the flexible degree of freedom of the topside and hull, especially surge and sway, small peaks are observed around the frequency ratio β = 1, which corresponds to resonance. However, the major peak lies outside the resonance zone, indicating that these responses are primarily affected by non-resonance effects. Specifically, these effects are wave-induced and occur under peak wave conditions. This phenomenon is possible because the natural periods of the flexible degrees of freedom are well outside the wave period zone. By contrast, the stiff degrees of freedom, such as deck heave, roll, and pitch, demonstrate considerable resonance response, as evidenced by the major peak around β = 1. This finding is due to the overlap between wave frequency and the natural structural frequencies for these degrees of freedom. Interestingly, the buoyant leg pitch response shows a major peak outside the resonance window, indicating that its characteristics substantially vary from the deck pitch. While the pitch of the legs is wave-induced, the deck pitch is attributed to other factors, such as the differential heave of the legs. Differential heave occurs when the heave motion

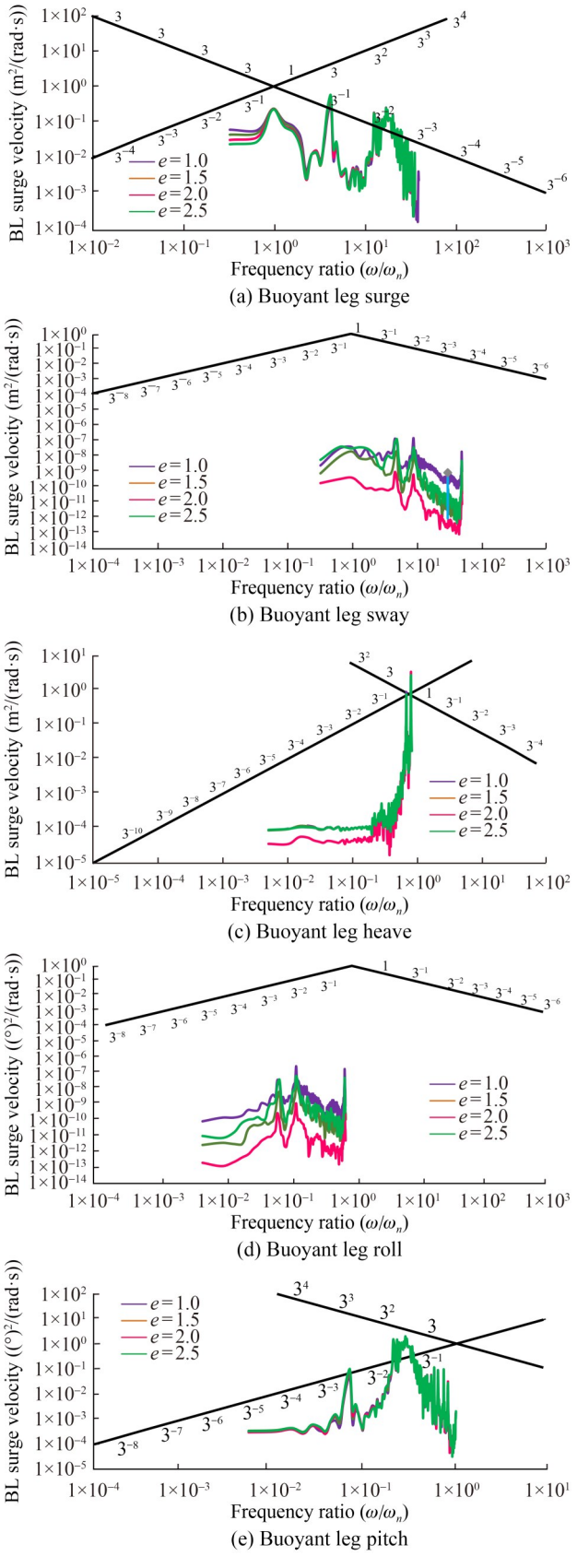

Figure 7 Four-way logarithmic buoyant leg responses during rocket launch for various elliptical legs

Table 7 Comparison of the buoyant leg responses for various elliptical legs

Leg eccentricity	Buoyant leg responses				
	Surge	Sway	Heave	Roll	Pitch
Circular ($e = 1$)	Max (1)	Max (1)	Max	Max (1)	Max
$e = 1.5$	2	3	Max	3	Max
$e = 2$	3	Min (4)	Min (4)	Min (4)	Max
$e = 2.5$	Min (4)	2	Max	2	Max

of three legs differs from each other. The eccentric rocket launch also contributes to deck pitch, a motion that is not transferred to the legs due to the ball and socket joints.

Analysis of the quadra-log plots for the flexible degrees of freedom of the deck and buoyant legs—specifically surge and sway—reveals small peaks around the frequency ratio $\beta = 1$, corresponding to resonance. However, the primary peak occurs outside the resonance zone, indicating that these responses are mainly influenced by non-resonance effects, particularly wave-induced forces during peak wave conditions. This finding can be attributed to the fact that the natural periods of these flexible degrees of freedom fall well outside the wave period range. By contrast, the stiff degrees of freedom, such as deck heave, roll, and pitch, exhibit pronounced resonance responses, as indicated by the major peak around $\beta = 1$. This finding is due to the overlap of wave frequencies with the natural structural frequencies for these degrees of freedom. Notably, the buoyant leg pitch response also shows a major peak outside the resonance window, emphasizing its distinct characteristics from the deck pitch. While the pitch response of the hull is influenced by metocean-induced forces, the deck pitch is affected by other factors, such as differential heave between the legs. Differential heave occurs when the heave motions of the three legs vary from one another. Additionally, the eccentric rocket launch induces deck pitch, a motion that is not transferred to the legs due to the ball and socket joints.

3.2 Force analyses on deck and buoyant legs

Figures 8 and 9, along with Tables 8 and 9, present the force power spectral density for the topside and hull of the structure. The study reveals that while surge force remains consistent across all buoyant leg configurations, the minimum sway force and roll moment on the deck occur with legs of eccentricity 2. The highest leg eccentricity results in the lowest deck pitch moment, whereas the circular cross-section exhibits the lowest deck heave force. Similarly, for the buoyant legs, surge force and pitch moment are consistent across all cases, with eccentricity 2 registering the minimum sway force and roll moment. As with the deck, the lowest heave force is observed for the circular leg cross-section.

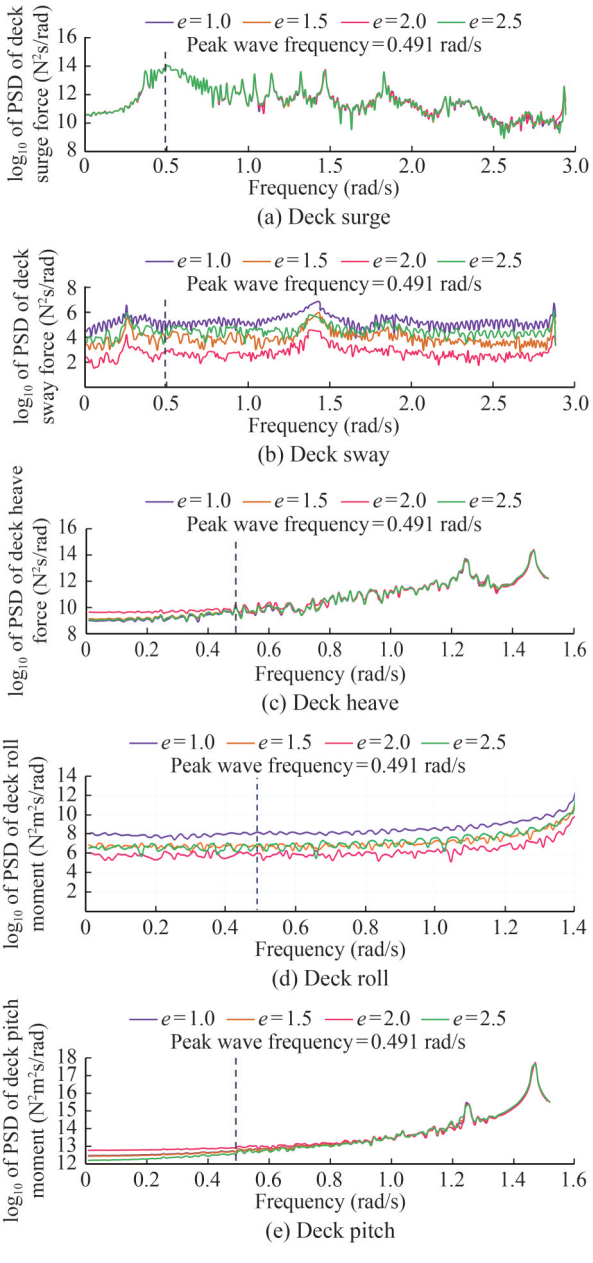

Figure 8 Deck forces during rocket launch for various elliptical legs

The surge force on the deck reaches its maximum at the peak wave frequency, while maximum sway occurs outside this zone, indicating that sway force is influenced by the wake region, which is particularly prominent in circular cross-sections compared to highly eccentric ellipses. The deck and leg pitch moments exhibit different characteristics. The deck pitch moment peak is more than five times smaller than the leg pitch moment. Additionally, the deck pitch moment peak occurs outside the peak wave zone, indicating it is due to rocket thrust force and differential heave of the legs. By contrast, the peak leg pitch moment, driven by wave impacts, occurs within the peak wave zone. The clear interaction between leg heave and deck pitch is

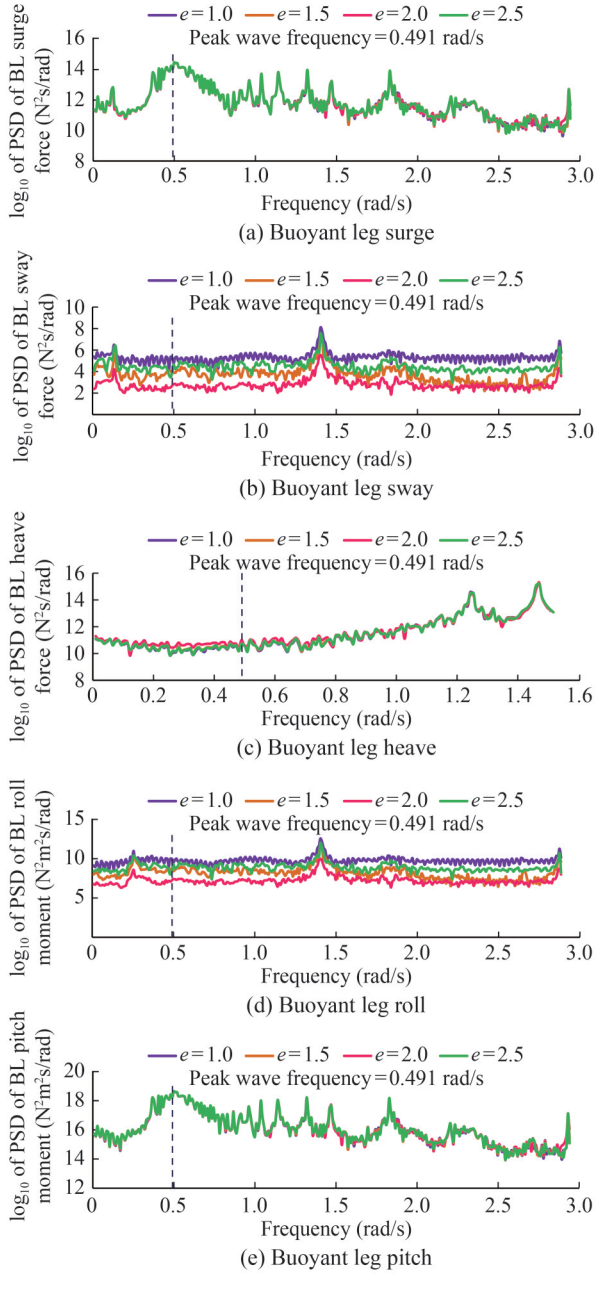

Figure 9 Buoyant leg forces during rocket launch for various elliptical legs

Table 8 Comparison of the deck forces for various elliptical legs

Leg eccentricity	Deck forces				
	Surge	Sway	Heave	Roll	Pitch
Circular (e = 1)	Max	Max (1)	Min (4)	Max (1)	3
e = 1.5	Max	3	2	2	2
e = 2	Max	Min (4)	Max (1)	Min (4)	Max (1)
e = 2.5	Max	2	3	3	Min (4)

evident from the striking similarity observed in their respective force and moment spectra. Furthermore, the leg pitch moment spans a wide frequency band, while the deck pitch moment is concentrated within a narrow band. This finding illustrates that the deck pitch behaves as a quasi-static process, while the leg pitch is dynamic. These results have substantial engineering and scientific implications. To minimize the deck pitch moment, limiting the transfer of differential heave forces to the deck is necessary.

Table 9 Comparison of the buoyant leg forces for various elliptical legs

Leg eccentricity	Buoyant leg forces				
	Surge	Sway	Heave	Roll	Pitch
Circular (e = 1)	Max	Max (1)	Min	Max (1)	Max
e = 1.5	Max	3	Min	3	Max
e = 2	Max	Min (4)	Max (1)	Min (4)	Max
e = 2.5	Max	2	Min	2	Max

3.3 Effect of rocket launch angle

The oblique launch analysis, which varied the rocket launch angle from 30° to 150°, shows that the structure's displacement increases during the rocket launch. The parametric curves illustrate the time variation of relative displacement for each degree of freedom. Relative displacement is defined as the difference between the instantaneous structural displacements during the rocket launch and those observed under non-launch conditions. The numerical simulation of the launch occurs at t = 200 s; hence, relative displacement becomes apparent only after this time. These curves generally highlight the impact of the marine launch on the structural response. The results, detailed in Tables 10–13, reveal an oscillatory behavior in the relative displacements, indicating that the seaborne launch does not substantially affect the mean response. This finding is further confirmed by the data, revealing that the mean relative response remains well below 1% of the total response. The minimal change in the mean response after the launch indicates that the platform retains its capability to re-center itself.

Table 10 Statistics of the deck response without launch

Statistics	Surge (m)	Heave (m)	Pitch (°)
Max	24.63	0	0.18
Min	0	−0.29	−0.18
Mean	17.35	−0.09	−0.01
SD	2.90	0.03	0.06

The relative deck surge response amplitude was −0.23% and 0.22% for A30 and A150, respectively, and negligible at −0.01% for A90. This finding demonstrates that the vertical launch has the least effect on the surge response of the Triceratops, while oblique launches induce a slight

Table 11 Statistics of the change in deck response for various launch angles (as the % of response without launch)

Types of launch	Statistics	Surge (m)	Heave (m)	Pitch (°)
A30	Max	1.49	–	8.27
	Min	–	3.14	7.98
	Mean	−0.23	−0.33	−0.07
	SD	6.06	5.79	3.35
A60	Max	0.99	–	9.73
	Min	–	3.61	9.91
	Mean	−0.14	−0.21	−0.29
	SD	3.59	7.04	7.49
A90	Max	0.24	–	13.81
	Min	–	3.30	13.75
	Mean	−0.01	−0.03	−0.45
	SD	0.56	7.29	10.36
A120	Max	2.07	–	16.16
	Min	–	3.62	15.86
	Mean	0.13	0.17	−0.47
	SD	3.37	7.00	10.85
A150	Max	3.65	–	15.92
	Min	–	3.62	15.55
	Mean	0.22	0.17	−0.38
	SD	5.95	7.01	10.54

Table 12 Statistics of the buoyant leg (BL) response

Statistics	Surge (m)	Heave (m)	Pitch (°)
Max	21.39	0	2.87
Min	0	−0.31	−1.42
Mean	16.04	−0.16	0.50
SD	2.51	0.05	0.49

deviation in the mean surge response. The relative deck heave response amplitude is −0.33% and 0.17% for A30 and A150, respectively, and negligible at −0.03% for A90. Paradoxically, the vertical launch, which exerts the largest downward thrust, demonstrates the smallest change in the heave mean. This finding primarily indicates that the heave is not directly caused by the vertical thrust force but rather by the motion of the topside along the *x*-axis. Hence, a surge–heave coupling effect exists for the Triceratops deck, as evidenced by the similar behavior in the surge and heave relative mean values. Second, this finding affirms the vertical stiffness of the structure, which resists the vertical thrust applied to the deck. The relative deck pitch response amplitude is −0.07% and −0.38% for A30 and A150, respectively, and −0.45% for A90. The negative sign indicates that the rotation is anti-clockwise. The highest relative mean occurs for the vertical launch (A90) due to the largest thrust-lever arm effect. Furthermore, the maximum and minimum relative values for heave and pitch are the lowest when the rockets are launched at 30° (Figure 10).

Regarding the leg displacements, the relative surge amplitude is −0.22%, 0.21%, and −0.01% for A30, A150, and A90, respectively. The relative heave amplitude is −0.17% and 0.18% for A30 and A150, respectively, and negligible for A90 (Figure 11). The exact similarity in deck surge and heave behavior is due to the translationally

Table 13 Statistics of the change in buoyant leg response for various launch angles (as the % of response without launch)

Types of Launch	Statistics	Surge (m)	Heave (m)	Pitch (°)
A30	Max	1.41	–	1.34
	Min	–	2.71	3.29
	Mean	−0.22	−0.17	−0.30
	SD	6.48	4.86	1.59
A60	Max	0.96	–	0.83
	Min	–	5.62	1.97
	Mean	−0.13	−0.10	−0.18
	SD	3.85	7.35	0.95
A90	Max	0.27	–	0.14
	Min	–	7.65	0.30
	Mean	−0.01	0.00	−0.01
	SD	0.60	9.20	0.19
A120	Max	2.14	–	0.95
	Min	–	8.29	1.44
	Mean	0.12	0.11	0.16
	SD	3.60	9.54	0.95
A150	Max	3.77	–	1.57
	Min	–	8.54	2.47
	Mean	0.21	0.18	0.29
	SD	6.36	9.09	1.57

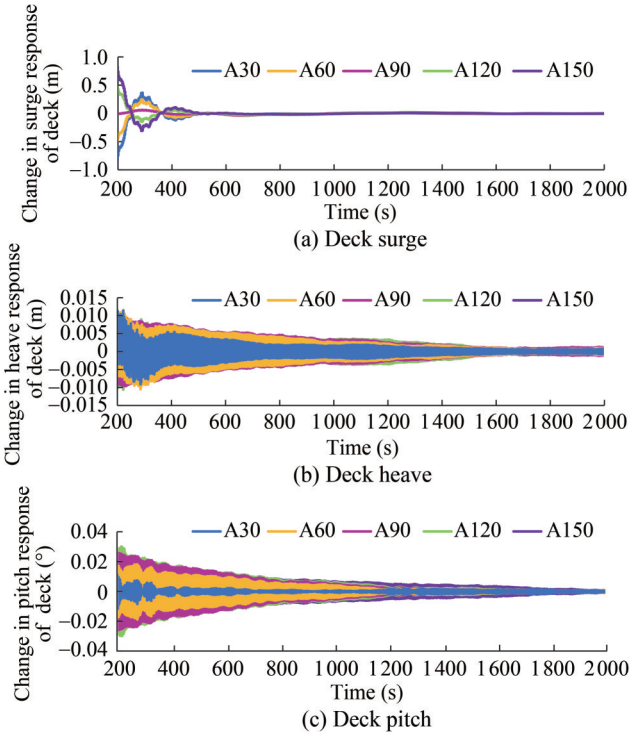

Figure 10 Variation in relative deck responses for various launch angles

rigid connection between the topside and the hull. The relative pitch amplitude is −0.30% and 0.29% for A30 and A150, respectively, and −0.01% for A90. The distinct pitch motion response of the Triceratops is marked by differences between the behavior of the buoyant legs and the deck.

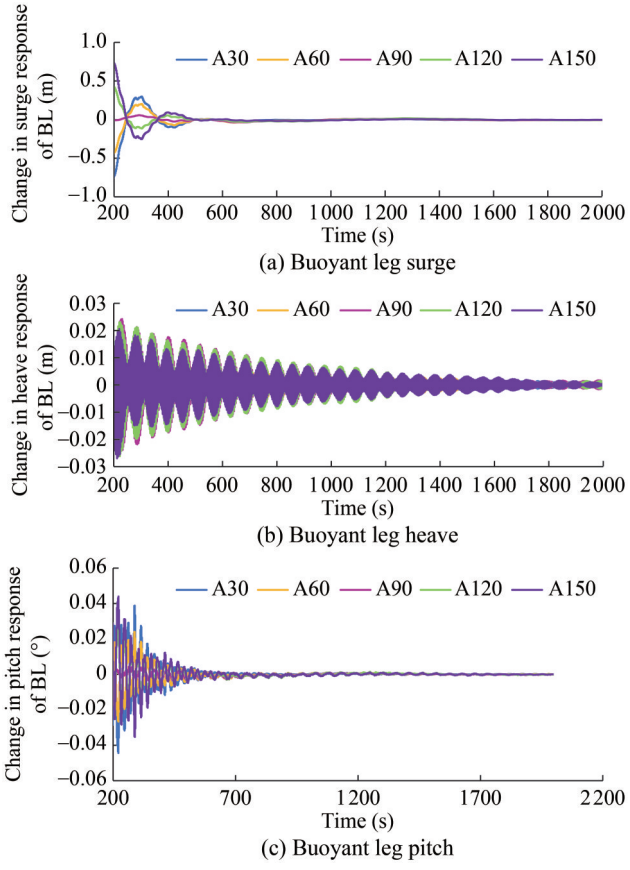

Figure 11 Variation in relative buoyant leg (BL) responses for various launch angles

Additionally, the absolute pitch motion of the legs is substantially larger than that of the deck. While the waves exert moments on the legs, causing them to pitch, this motion is not transferred to the deck, resulting in a low pitch motion. Therefore, although the percentage change in pitch motion caused by the launch is similar for the deck and the legs, the absolute magnitude of pitch motion is considerably larger for the legs due to their initially higher wave-induced pitch response.

3.4 Impact of oblique launch

The oblique launch notably amplifies the forces exerted on the deck in the heave and pitch (Figure 12 and Tables 14–15); however, the extent of this increase varies with each launch angle. For the case A150, the heave force and pitch moment on the deck exhibit low peak values. The graphs show that the launch forces cause an oscillatory pattern in

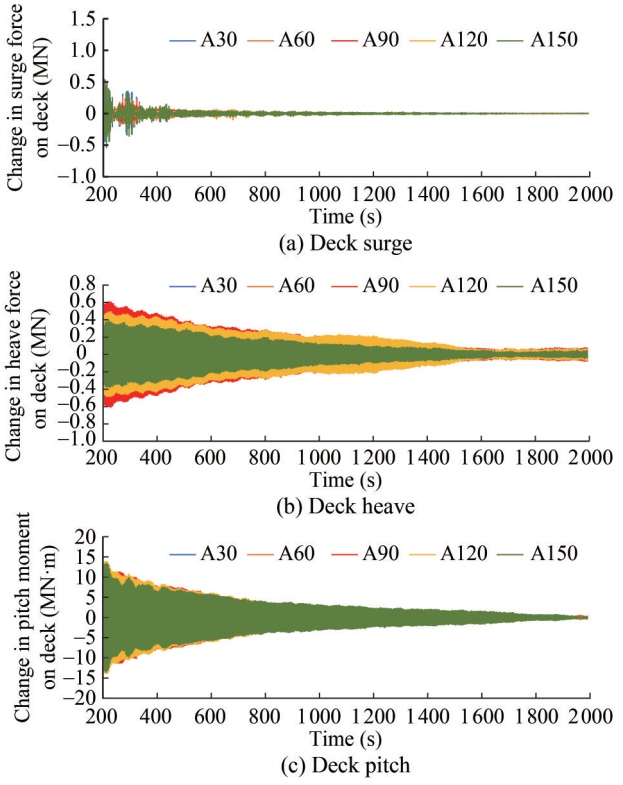

Figure 12 Variation in relative deck forces for various launch angles

Table 14 Statistics of the deck force without launch

Statistics	Surge (MN)	Heave (MN)	Pitch (MN·m)
Max	37.33	4.51	71.77
Min	−25.00	−4.36	−73.00
Mean	−0.01	0.00	−0.01
SD	7.01	2.08	26.16

the force–time history. Similar to the responses, these forces persist over an extended period, making fatigue analysis a crucial aspect during the design phase of the Triceratops.

The relative deck surge force mean for A30–A150 is less than 1%. The relative deck heave force for A30, A60, A90, A120, and A150 is −0.22%, −1.74%, −2.79%, −1.96%, and −1.49%, respectively. This finding indicates that the highest variation occurs during the vertical launch, while the lowest variation is observed for A30. Concerning the pitch, the highest value is recorded for A60 at 2.95%, while the lowest occurs for A90 at 0.95%.

The wave-induced moments on the legs average 11 MN m, with a maximum of 1 790 MN m, while the corresponding values for the deck are 0.01 and 72 MN m (Figure 13 and Tables 16–17). This beneficial outcome is attributed to the innovative joint design of the ball and socket joint, which prevents the transmission of moments and rotations from the legs to the deck. From a structural engineering perspective, this outcome is advantageous because offshore platforms are designed based on strength criteria.

Table 15 Statistics of the change in deck force for various launch angles (as the % of forces without launch)

Types of Launch	Statistics	Surge (MN)	Heave (MN)	Pitch (MN·m)
A30	Max	2.23	9.86	9.16
	Min	3.60	10.15	11.01
	Mean	−0.15	−0.22	1.18
	SD	1.27	5.40	3.50
A60	Max	1.29	12.70	12.00
	Min	2.09	12.98	17.80
	Mean	−0.22	−1.74	2.95
	SD	0.79	7.93	8.41
A90	Max	0.43	13.51	17.18
	Min	0.56	17.02	20.54
	Mean	−0.18	−2.79	0.95
	SD	0.37	8.66	11.68
A120	Max	1.38	10.98	19.44
	Min	1.86	18.36	19.17
	Mean	−0.08	−1.96	1.16
	SD	0.81	8.03	12.18
A150	Max	2.44	8.70	18.81
	Min	3.29	14.83	19.17
	Mean	0.01	−1.49	1.90
	SD	1.31	5.76	11.75

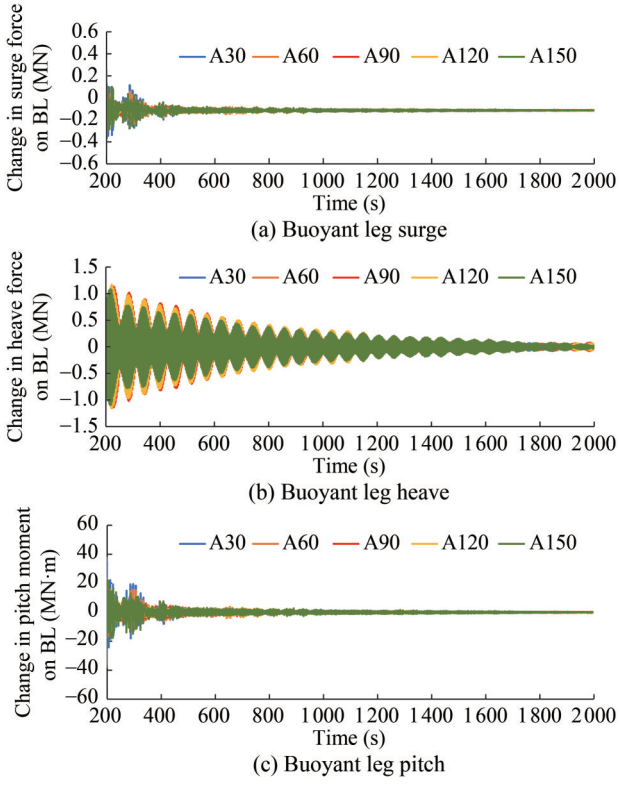

Figure 13 Variation in relative leg forces for various launch angles

Table 16 Statistics of the buoyant leg force

Statistics	Surge (MN)	Heave (MN)	Pitch (MN·m)
Max	18.45	6.18	1790.00
Min	−23.00	−6.13	−1600.00
Mean	−0.09	0.02	−11.00
SD	4.81	2.20	376.00

Table 17 Statistics of the change in buoyant leg force for various launch angles (as the % of forces without launch)

Types of Launch	Statistics	Surge (MN)	Heave (MN)	Pitch (MN·m)
A30	Max	2.52	8.97	2.20
	Min	1.97	9.09	2.87
	Mean	−0.01	0.03	−0.01
	SD	0.88	4.48	1.15
A60	Max	1.47	14.07	1.28
	Min	1.15	14.16	1.68
	Mean	−0.01	0.03	−0.02
	SD	0.55	8.04	0.73
A90	Max	0.36	18.38	0.46
	Min	0.31	18.51	0.40
	Mean	−0.01	−0.05	−0.02
	SD	0.22	10.40	0.31
A120	Max	1.37	18.87	1.48
	Min	1.15	18.82	1.37
	Mean	−0.01	−0.02	−0.01
	SD	0.52	10.68	0.69
A150	Max	2.41	17.45	2.62
	Min	2.02	17.74	2.43
	Mean	−0.00	0.01	−0.01
	SD	0.87	9.93	1.14

3.5 Impact of launch eccentricity

The second parametric study is conducted to analyze the effect of the launch eccentricity on the response of the Triceratops. Four cases are investigated, with eccentricities of 0, 10, 20, and 30 m, denoted as E0, E10, E20, and E30, respectively. A negligible change in the pitch response is observed when the vertical launch is conducted directly above the center of gravity of the deck. However, for E10, E20, and E30, the pitch response consistently increases to 0.14%, 0.29%, and 0.45% (Figure 14 and Table 18). This finding demonstrates that the cantilever effect of the eccentrical launch increasingly impacts the topside response about the sway axis. As expected, the buoyant leg pitch exhibits a minimal change of 0.01%, remaining constant across all four cases (Figure 15 and Table 19). As discussed in Section 3.1, this phenomenon is due to the novel connection that integrates the deck with the hull. The deck and buoyant leg surge remain constant throughout the various eccentric launch cases, which is intuitive because the launch is vertical and does not exert any horizontal force component on the structure. Furthermore, while the pitch

moment on the deck increases with eccentricity, the deck surge force remains constant throughout the present parametric study (Figure 16). Concerning the force on the buoyant leg, the lowest surge, heave, and pitch forces occur during the zero eccentricity launch (Figure 17).

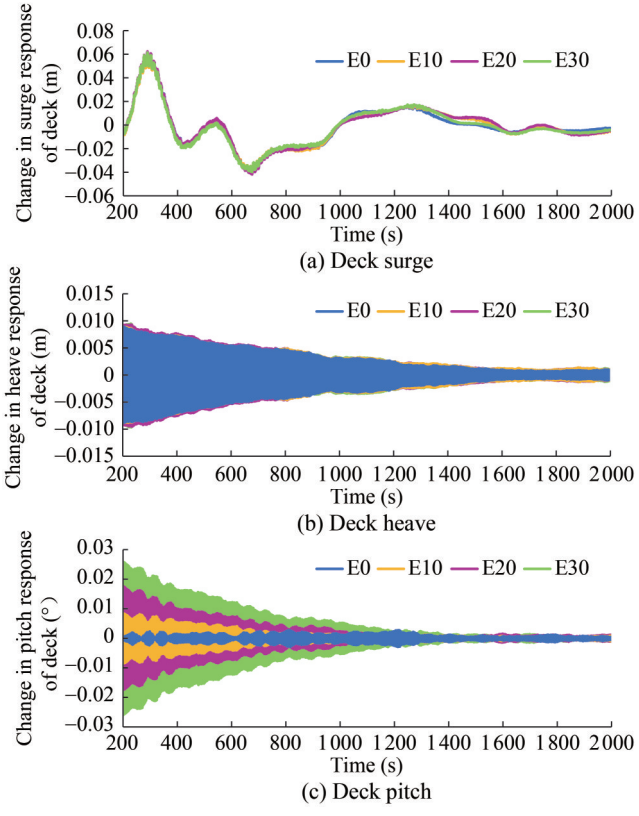

Figure 14 Variation in relative deck responses for various launch eccentricities

Table 18 Statistics of the change in deck response for various launch eccentricities (as the % of response without launch)

Types of Launch	Statistics	Surge (m)	Heave (m)	Pitch (°)
E0	Max	0.23	–	1.48
	Min	–	3.02	1.51
	Mean	−0.01	−0.03	0.00
	SD	0.55	7.07	1.51
E10	Max	0.23	–	4.50
	Min	–	3.03	4.49
	Mean	−0.01	−0.03	−0.14
	SD	0.55	7.13	3.19
E20	Max	0.25	–	9.36
	Min	–	3.26	9.28
	Mean	−0.01	−0.03	−0.29
	SD	0.57	7.42	6.39
E30	Max	0.24	–	13.81
	Min	–	3.30	13.75
	Mean	−0.01	−0.03	−0.45
	SD	0.55	7.29	10.36

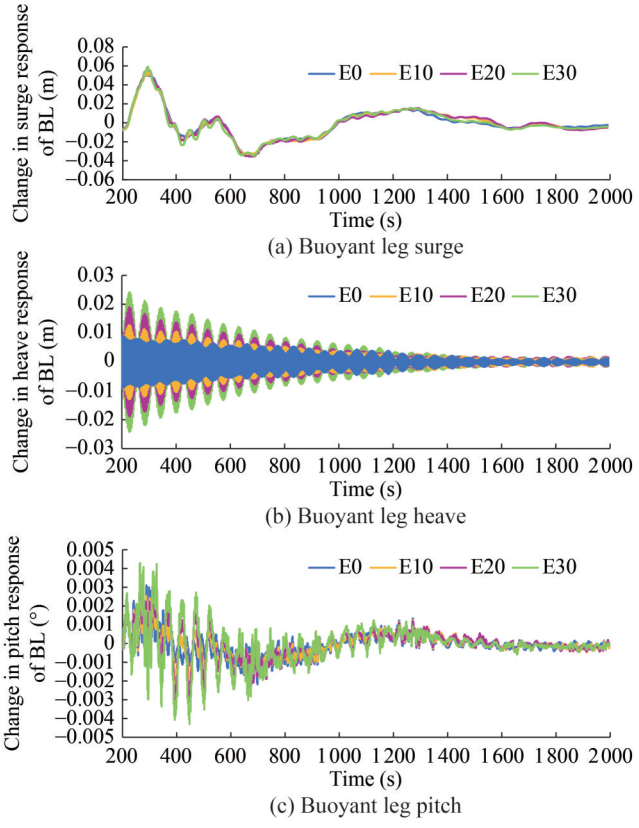

Figure 15 Variation in relative buoyant leg (BL) responses for various launch eccentricities

Table 19 Statistics of the change in buoyant leg response for various launch eccentricities (as the % of response without launch)

Types of launch	Statistics	Surge (m)	Heave (m)	Pitch (°)
E0	Max	0.24	–	0.11
	Min	–	2.86	0.15
	Mean	−0.01	−0.02	−0.01
	SD	0.59	5.08	0.12
E10	Max	0.25	–	0.11
	Min	–	4.06	0.15
	Mean	−0.01	−0.01	−0.01
	SD	0.59	5.51	0.12
E20	Max	0.27	–	0.13
	Min	–	5.99	0.21
	Mean	−0.01	−0.01	−0.01
	SD	0.61	7.01	0.15
E30	Max	0.27	–	0.14
	Min	–	7.65	0.30
	Mean	−0.01	0.0	−0.01
	SD	0.60	9.20	0.19

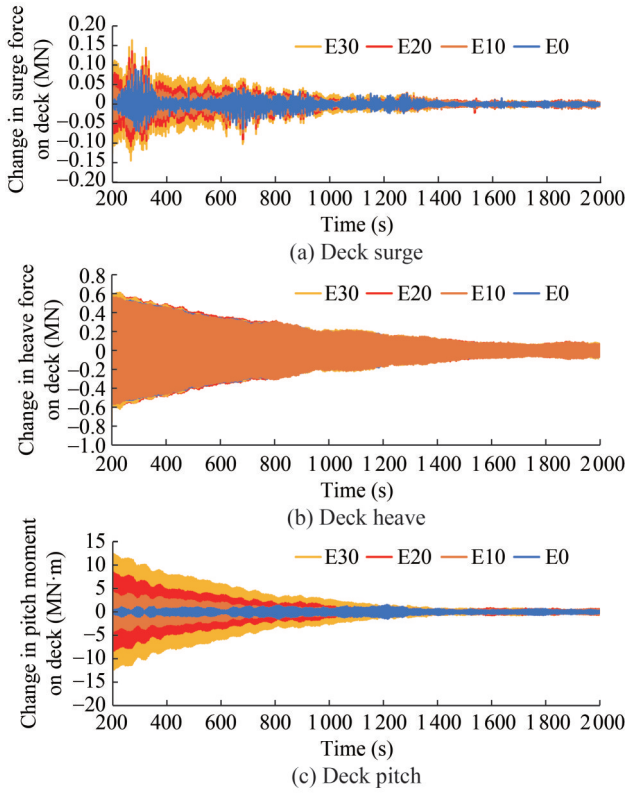

Figure 16 Variation in relative deck forces for various launch eccentricities

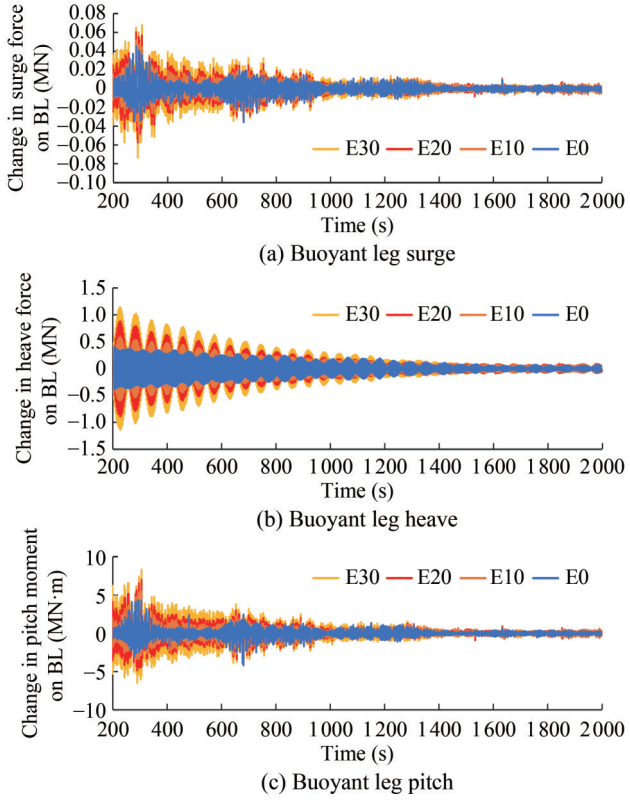

Figure 17 Variation in relative leg forces for various launch eccentricities

4 Conclusions

This study investigates the impact of using elliptical legs on the response and force characteristics of the rocket-launching Triceratops. In addition to standard circular legs, three distinct elliptical configurations are numerically analyzed. The study also explores how the launch angle and eccentricity influence the response characteristics of the deep-sea Triceratops. Dynamic analyses are performed with and without the rocket, considering various launch angles and eccentricities. Based on these analyses, the following conclusions are derived:

1) Circular legs experience maximum wave exposure in the surge direction, resulting in the highest surge response. They also register the highest sway due to the formation of a wake region. However, this phenomenon is counteracted by the wave impact on the sway axis, which is greatest for legs with the highest eccentricity. The optimal sway response is observed with legs having an eccentricity of 2.

2) The Triceratops with elliptical legs experienced less motion in surge, sway, heave, and roll of the deck. This finding is due to the innovative joint that integrates the hull with the topside, preventing the rotation from being transferred from the legs to the deck. The deck's pitch is primarily due to the uneven heave of the hull, which results from the dynamic variations in tether tension. Therefore, the pitch motion of the deck and legs is governed by different factors. From an engineering standpoint, controlling deck pitch is achieved by minimizing the differential heave of the legs.

3) The vertical launch has the least effect on the surge response of the Triceratops, showcasing the high vertical stiffness of the platform. The relative structural response amplifies when the rocket is launched, regardless of the launch angle or eccentricity. The vertical force exerted on the deck is at its maximum during a vertical launch and at its minimum when launched at 30°. The pitch moment on the deck increases with launch eccentricity, which is attributed to the cantilever action of the launch platform.

4) The wave-induced moment on the buoyant legs is substantially higher than that on the deck. However, the latter is more influenced by the moment induced by the rocket launch.

The study indicates that the pitch motion of the deck during the launch is most effectively controlled by employing elliptical legs with an eccentricity of 2. One of the primary limitations of the study lies in its focus on surge, sway, heave, roll, and pitch responses without considering the torsion, structural vibrations, and resonance effects of local structural elements that could influence the overall stability. Additionally, the effect of multidirectional waves, currents, and winds are excluded, which simplifies the model and may not fully capture real-world sea-state interactions. However, the impact of the rocket launch is com-

prehensively examined. The study also excludes the impact of heat generated during the rocket launch on the platform's mechanical properties, disregarding potential degradation in strength, stiffness, or elastic modulus due to thermal exposure. Furthermore, this study considered leg eccentricities of 1.0, 1.5, 2.0, and 2.5, with an eccentricity of 2.0 yielding the best overall performance in terms of motion response. However, the optimal eccentricity may vary depending on changes in hydrodynamic loads, tether forces, and platform mass distribution. The actual optimal leg eccentricity may not necessarily be 2. Future work should extend this analysis using optimization techniques and numerical methods to comprehensively assess the impact of leg eccentricity on platform behavior. Additionally, advanced optimization techniques should be developed and implemented to systematically refine design parameters and minimize leg heave differences, further enhancing the reduction of deck pitch response under dynamic loading conditions. The above limitations also emphasize the potential areas for future research, with the present study serving as a base reference.

Funding This research received a specific grant from the Prime Minister Research Fund to the second author (PMRF), Govt. of India (Grant ID: 2503484).

Competing interest The authors have no competing interests to declare that are relevant to the content of this article.

References

Ahmad F (2021a) Design of floating offshore platform. Islamic University of Technology, Gazipur, Bangladesh, Report No. Report-01. https://doi.org/10.13140/RG.2.2.10384.84486

Ahmad O (2021b) An overview of design, construction, and installation of gravity offshore platforms. International Journal of Advanced Engineering, Sciences and Applications 3(1): 27-32. https://doi.org/10.47346/ijaesa.v3i1.81

Amiri N, Shaterabadi M, Kashyzadeh R, Chizari M (2021) A comprehensive review of design, monitoring, and failure in fixed offshore platforms. Journal of Marine Science and Engineering 9(12): 1349. https://doi.org/10.3390/jmse9121349

Ashish PU, Chandrasekaran S, Giorgio S (2024) Parametric study on the deep ocean space-rocket launching Triceratops. Ocean Engineering 295: 116946. https://doi.org/10.1016/j.oceaneng.2024.116946

Buhrig AL, Cox SM, Alexander TM, Krenitsky DM, Huebner CC (1996) Sea launch program overview. American Institute of Aeronautics and Astronautics, Reston, United States, AIAA Technical Report No. AIAA-96-1186-CP

Caporale AJ (1968) History of San Marco. NASA, Washington, Report No.: NASA-TM-X-70523, X-724-70-19

Cashin LM (2001) Lessons from sea launch. Maxwell AFB: Air University, Alabama, USA, Report No.: AU/ACSC/039/2001-04

Chandrasekaran S, Madhuri S, Jain AK (2013) Aerodynamic response of offshore Triceratops. Ship and Offshore Structures 8(2): 123-140. https://doi.org/10.1080/17445302.2012.691271

Chandrasekaran S (2017) Dynamic analysis and design of ocean structures. 2nd edn, Springer, Singapore

Chandrasekaran S, Jain AK, Shafiq N, Wahab MMA (2021) Design aids for offshore platforms under special loads. CRC Press, Florida, 280

Chandrasekaran S, Madhuri S (2015) Dynamic response of offshore Triceratops: Numerical and experimental investigations. Ocean Engineering 109: 401-409. https://doi.org/10.1016/j.oceaneng.2015.09.042

Chandrasekaran S, Mayank S (2017) Dynamic analyses of stiffened Triceratops under regular waves: Experimental investigations. Ships and Offshore Structures 12(5): 697-705. https://doi.org/10.1080/17445302.2016.1200957

Chandrasekaran S, Nagavinothini R (2019) Parametric studies on the impact response of offshore Triceratops in ultra-deep waters. Structure and Infrastructure Engineering 16(7): 1002-1018. https://doi.org/10.1080/15732479.2019.1680707

Chandrasekaran S, Rao M (2019) Numerical analysis on Triceratops restraining system: failure conditions of tethers. International Journal of Environmental and Ecological Engineering 13(9): 588-592. DOI: 10.5281/zenodo.3461996

Chandrasekaran S, Shah B, Chauhan YJ (2023) Tether response of offshore Triceratops under hurricane conditions. Structures 51: 513-527. https://doi.org/10.1016/j.istruc.2023.03.059

Chauhan Y, Chandrasekaran S, Serino G, Sanghvi C, Gohil A (2024) Feasibility study of offshore triceratops-supported floating offshore wind turbine. J. Inst. of Engineers (India) Series A 105: 295-305. https://doi.org/10.1007/s40030-024-00800-w

Chen Y, Zhang D (2017) Response-based analysis for Tension Leg Platform. J. Marine Sc. and App. 16(1): 87-92. https://doi.org/10.1007/s11804-017-1390-1

Drain J (1993) Sea-launch for small satellites: an American/Russian joint venture. Proceedings of the 7th Annual. AIAA/USU Conference on Small Satellites, Logan, Utah, USA

Frieze PA, Morandi AC, Birkinshaw M, Smith D, Dixon AT (1997) Fixed and jack-up platforms: Basis for reliability assessment. Marine Structures 10(2-4): 263-284. https://doi.org/10.1016/S0951-8339(97)00001-4

Fu JY, Peng DJ, Xiong XD, Jia H (2018) Hydrodynamic performance of semi-submersible sea-launching platform. Ship Engineering 40(12): 73-76. (in Chinese)

Jain AK (1997) Nonlinear coupled response of offshore tension leg platforms to regular wave forces. Ocean Engineering 24(7): 577-592. https://doi.org/10.1016/0029-8018(95)00059-3

Johnson CP, Mekba BB, Roesset JM (1993) Simplified modeling for the nonlinear response of tension leg platforms in deep water. Proceedings of the Third International Offshore and Polar Engineering Conference, Singapore, 326-333

Li R, Ge H, Shu G (2017) Parametric study on seismic control design of a new type of SMA damper installed in a frame-type bridge pier. Journal of Aerospace Engineering 31(2): 04017100. https://doi.org/10.1061/(ASCE)AS.1943-5525.0000809

Li Y, Hu Z (2022) A review of multi-attributes decision-making models for offshore oil and gas facilities decommissioning. Journal of Ocean Engineering and Science 7(1): 58-74. https://doi.org/10.1016/j.joes.2021.05.002

Li Y, Kareem A (1992) Response of tension leg platform to wave drift forces. Proceedings of the Offshore Technology Conference, Houston, Texas, OTC-6885-MS

Lin BC, Tadjbakhsh IG, Papageorgiou AS, Ahmadi G (1990) Performance of earthquake isolation systems. Journal of

Engineering Mechanics 116(2): 24383. https://doi.org/10.1061/(ASCE)0733-9399(1990)116:2(446)

Mazzaretto OM, Menéndez M, Lobeto H (2022) A global evaluation of the JONSWAP spectra suitability on coastal areas. Ocean Engineering 266: 112756. https://doi.org/10.1016/j.oceaneng.2022.112756

Nagavinothini R, Chandrasekaran S (2020) Dynamic response of offshore Triceratops with elliptical buoyant legs. Innovative Infrastructure Solutions 5(2): 697-705. https://dx.doi.org/10.1007/s41062-020-00298-8

Newmark NM (1959) A method of computation for structural dynamics. Journal of Engineering Mechanics ASCE 85(3): 67-94. https://doi.org/10.1061/JMCEA3.0000098

Pang F, Qin Y, Tang Y, Gao C, Li H (2023) Experimental study on impact response of sea-borne rocket launch platform. Ocean Engineering 280: 114623. https://doi.org/10.1016/j.oceaneng.2023.114623

Seumahu ES (1997) Exploration of the equatorial LEO orbit for communication and other applications. In: Haskell G, Rycroft M (Eds.). Space of service to humanity. Springer, Dordrecht

Shabanlou M, Moghaddam H, Saedi Daryan A (2021) The effect of geometry on structural behavior of buildings with steel plate shear wall system subjected to blast loading. International Journal of Steel Structures 21: 650-665. https://doi.org/10.1007/s13296-021-00463-4

Song Z, Xie Z, Qiu L, Xiang D, Li J (2021) Prospects of sea launches for Chinese cryogenic liquid-fueled medium-lift launch vehicles. Chinese Journal of Aeronautics 34(1): 424-437. https://doi.org/10.1016/j.cja.2020.06.018

White CN, Copple RW, Capanoglu C (2005) Triceratops: An effective platform for developing oil and gas fields in deep and ultra-deep water. Proceedings of the International Offshore and Polar Engineering Conference, Seoul, Korea, 133-139

Zhang T, Li L (2021) Analytical analysis for optimizing mass ratio of nonlinear tuned mass dampers. Nonlinear Dynamics 106: 1955-1974. https://doi.org/10.1007/s11071-021-06845-x